



Thermomechanical milling of accessory lithics in volcanic conduits



Michelle E. Campbell^a, James K. Russell^{a,*}, Lucy A. Porritt^b

^a *Volcanology & Petrology Laboratory, Department of Earth, Ocean and Atmospheric Sciences, University of British Columbia, Vancouver, V6T 1Z4, Canada*

^b *Department of Earth Sciences, University of Bristol, Clifton, BS8 1RJ, UK*

ARTICLE INFO

Article history:

Received 20 April 2013

Received in revised form 18 June 2013

Accepted 5 July 2013

Available online 29 July 2013

Editor: T. Elliot

Keywords:

volcanology
accessory lithic
milling
morphology
ash-blasting
Mount Meager

ABSTRACT

Accessory lithic clasts recovered from pyroclastic deposits commonly result from the failure of conduit wall rocks, and represent an underutilized resource for constraining conduit processes during explosive volcanic eruptions. The morphological features of lithic clasts provide distinctive ‘textural fingerprints’ of processes that have reshaped them during transport in the conduit. Here, we present the first study focused on accessory lithic clast morphology and show how the shapes and surfaces of these accessory pyroclasts can inform on conduit processes. We use two main types of accessory lithic clasts from pyroclastic fallout deposits of the 2360 B.P. subplinian eruption of Mount Meager, British Columbia, as a case study: (i) rough and subangular dacite clasts, and (ii) variably rounded and smoothed monzogranite clasts. The quantitative morphological data collected on these lithics include: mass, volume, density, 2-D image analysis of convexity (C), and 3-D laser scans for sphericity (Ψ) and smoothness (S). Shaping and comminution (i.e. milling) of clasts within the conduit are ascribed to three processes: (1) disruptive fragmentation due to high-energy impacts between clasts or between clasts and conduit walls, (2) ash-blasting of clasts suspended within the volcanic flux, and (3) thermal effects. We use a simplified conduit eruption model to predict ash-blasting velocities and lithic residence times as a function of clast size and source depth, thereby constraining the lithic milling processes. The extent of shape and surface modification (i.e. rounding and honing) is directly proportional to clast residence times within the conduit prior to evacuation. We postulate that the shallow-seated dacite clasts remain subangular and rough due to short (<2 min) residence times, whereas monzogranite clasts are much more rounded and smoothed due to deeper source depths and consequently longer residence times (up to ~1 h). Larger monzogranite clasts are smoother than smaller clasts due to longer residence times and to greater differential velocities within the ash-laden jet. Lastly, our model residence times and mass loss estimates for rounded clasts are used to estimate minimum attrition rates due to volcanic ash-blasting within the conduit (e.g., $12 \text{ cm}^3 \text{ s}^{-1}$ for 25 cm clasts, sourced at 2500 m depth).

© 2013 Elsevier B.V. All rights reserved.

1. Introduction

Accessory lithic clasts recovered from pyroclastic fallout deposits are an underutilized resource for understanding the processes operating in volcanic conduits during explosive eruptions. Lithic clasts result from syn-eruptive fragmentation of conduit wall rocks and are entrained into the rapidly ascending stream of erupting material. Here, we use the size, morphology and textural properties of accessory lithic clasts to elucidate the “milling” processes operating in volcanic conduits during explosive eruptions.

The pyroclastic fallout deposit of the 2360 B.P. eruption of the Mount Meager Volcanic Complex in British Columbia, Canada (Fig. 1), contains two main types of accessory lithic clasts: (i) rough and subangular dacite clasts, and (ii) smooth and rounded monzogranite clasts. Milled or highly rounded accessory lithics have

been reported in many other pyroclastic deposits; examples include Santorini (Mellors and Sparks, 1991), the Meidob volcanic field in Sudan (Franz et al., 1997), the Kaingaroa ignimbrites of New Zealand (Nairn et al., 1994), and the Kos Plateau Tuff, Greece (Allen and Cas, 1998). Nairn et al. (1994) observed that the largest lithics in the Kaingaroa ignimbrites were typically the roundest, and suggested that they were shaped through repeated fall back and milling in the vent(s). Mellors and Sparks (1991) noted that many of the rounded lithics at Santorini display concentric rinds of altered rock, and attributed the rounding of these lithics to the abrasion of these fragile rinds during eruption and transport. To date, however, there have been no detailed studies of the processes or timescales associated with the volcanic milling of lithic clasts.

Here, we have used a variety of techniques, including 2-D image analysis and 3-D laser scanning, to describe and quantify the morphological properties of accessory lithic clasts recovered from the Mount Meager 2360 B.P. fallout deposits. Our analysis of these datasets suggests three main processes control clast size, shape

* Corresponding author. Tel.: +778 995 7710; fax: +604 822 6088.

E-mail address: krussell@eos.ubc.ca (J.K. Russell).

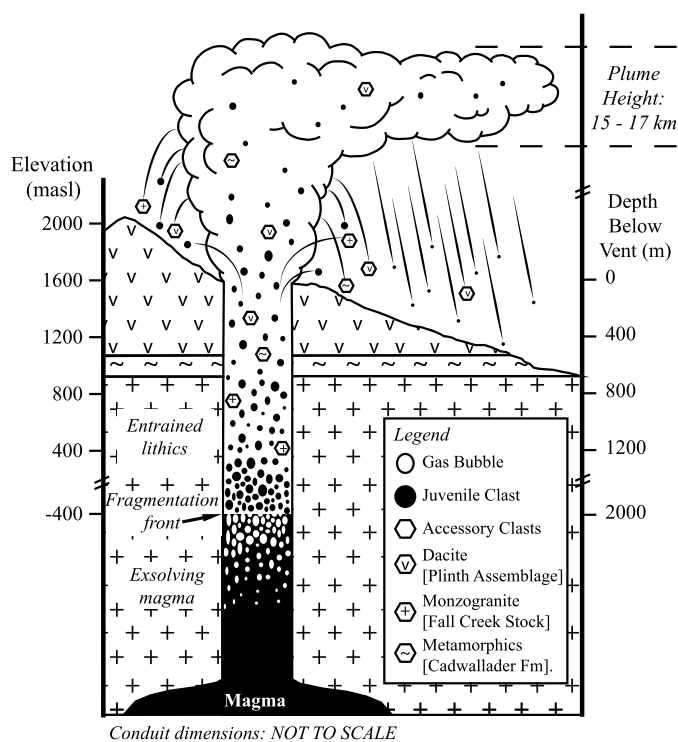


Fig. 1. Schematic cross-section through the conduit of the 2360 B.P. eruption of Mount Meager illustrating the country rock stratigraphy and source locations for the accessory lithic clasts found in fallout deposits. The fragmentation surface is likely to have varied in time but propagated to depths well in excess of 700–800 m below the vent (see text). Vertical conduit dimensions are to scale; horizontal scale is schematic.

and surface properties: (1) disruptive fragmentation (e.g., Dufek et al., 2012), (2) “ash-blasting” (i.e. sandblasting by volcanic ash), and (3) thermal effects. We conclude our study with a model for the comminution and reshaping of accessory lithic pyroclasts during explosive volcanic eruptions that constrains the mean diameter of the volcanic conduit, relates the shape and smoothness of individual clasts to residence time within the volcanic conduit, and establishes the amounts and rates of clast attrition.

2. Field site: the Mount Meager Volcanic Complex

The Mount Meager Volcanic Complex (MMVC) is a calc-alkaline volcanic complex located in southwestern British Columbia, Canada, at the northernmost extent of the Cascade Volcanic Arc (Green et al., 1988; Read, 1990; Sherrod and Smith, 1990). The MMVC consists of a number of partially overlapping volcanoes which produced pyroclastic deposits, lava flows and domes, and rock avalanche deposits from >1.9 Ma to recent times (Read, 1977a, 1977b). The youngest eruption of the MMVC is dated at 2360 B.P. (Clague et al., 1995) and produced the Pebble Creek Formation (PCF). The PCF deposits are predominantly dacitic in composition, and their geology is described in detail elsewhere (Hickson et al., 1999; Michol et al., 2008; Read, 1977a, 1977b, 1990; Stasiuk et al., 1996; Stewart et al., 2002, 2008).

The subplinian phase of the 2360 B.P. eruption (VEI = 4) generated a plume 15–17 km in height, and formed pumiceous pyroclastic fallout deposits totaling $\sim 4.2 \times 10^8 \text{ m}^3$ in volume (Andrews et al., in preparation; Hickson et al., 1999). The fallout deposits mantle the slopes of the mountainous terrain towards the northeast of the MMVC. Vent-proximal deposits of this tephra reach thicknesses of $\sim 80 \text{ m}$ (Hickson et al., 1999); very fine-grained, thin distal layers of the ash are identified in Alberta $\sim 500 \text{ km}$ distance from the vent (Nasmith et al., 1967; Westgate and Dreimanis, 1967).

The fallout deposits are unconsolidated, well-sorted and clast-supported, and comprise mainly juvenile, white to cream-colored pumice clasts. There are four main types of accessory lithic clasts within the fallout deposits (Campbell, 2012; Stasiuk et al., 1996; Stewart, 2002). This research focuses on the properties of the two most abundant types: grey, porphyritic dacite (Plinth Assemblage), and pale-pink, medium- to coarse-grained monzogranite (Fall Creek Stock) (Fig. 1). The accessory lithic clasts originate from country rock underlying the vent and source depths are estimated from surficial geology and drill hole data (Campbell, 2012).

3. Methodology

3.1. Sample collection

Monzogranite and dacite accessory lithic clasts from the PCF fallout deposits were recovered from two localities. A total of 109 monzogranite and 39 dacite lithics, ranging in size from 6 to $\sim 20,000 \text{ cm}^3$ and from 29 to $\sim 12,000 \text{ cm}^3$, respectively (Supplementary Appendix A), were sourced from proximal fallout deposits situated in the Great Pacific Pumice quarry $\sim 2 \text{ km}$ north of the 2360 B.P. vent ($50^\circ 40' 54'' \text{ N}$, $123^\circ 30' 43'' \text{ W}$). Another 51 monzogranite and 42 dacite lithics, ranging in size from 0.1 to 20 cm^3 and from 0.2 to 123 cm^3 , respectively (Supplementary Appendix A), were collected from an outcropping of fallout deposit $\sim 4 \text{ km}$ east-northeast of the vent ($50^\circ 40' 15'' \text{ N}$, $123^\circ 27' 16'' \text{ W}$). The relative abundances of lithics in the latter deposit is $\sim 4 \text{ wt.}\%$ dacite, $\sim 2 \text{ wt.}\%$ monzogranite, and $< 2 \text{ wt.}\%$ for other lithics (Campbell, 2012). These abundances probably overestimate the total volume of accessory lithics contained within the fallout deposit because of the vent proximal nature of these outcrops (e.g., Varekamp, 1993).

Clast volume (V) was calculated from measured values of mass and density using the Archimedes wet-dry technique (e.g., Hutchison, 1974). The mean densities of the monzogranite and dacite sample sets are $2.59 \pm 0.01 \text{ g/cm}^3$ and $2.47 \pm 0.10 \text{ g/cm}^3$, respectively (Supplementary Appendix A). Representative samples, spanning a range of sizes, for the two clast types are shown in Fig. 2.

3.2. Qualitative morphological analysis

The dacite lithics are subangular, equant to slightly elongate in form, and feature rough surfaces commonly bounded by prominent, or sharp, edges (Fig. 2b). A substantial number of dacite clasts feature one or more relatively smooth, planar, sometimes oxidized, surfaces that clearly originated as cooling joint surfaces (i.e. columnar jointing; Fig. 3c). Conversely, the monzogranite clasts are generally rounded to subrounded, and equant to elongate in form (Fig. 2a); larger clasts are commonly ellipsoidal in shape and their overall roundness and smoothness increases with increasing clast size. Some honed monzogranite clast surfaces feature concentric, partially detached, mm-scale flakes. Monzogranite clasts sometimes host two distinct surface types where the smooth, rounded exterior surfaces are truncated by relatively rough and planar surfaces bounded by sharp edges (e.g., Fig. 3a). These latter faces represent relatively late (i.e. post smoothing) breakages of the milled monzogranite clasts, suggesting that many monzogranite clasts undergo disruptive collisions immediately prior to their ejection from the conduit. In several samples, the late fracture surfaces truncate the highly smoothed surface of a rounded monzogranite clast but have, themselves, been subsequently milled to varying degrees (e.g., Fig. 3b). On the basis of these observations, the monzogranite sample set was subdivided into two categories: (1) “intact” monzogranites, having $\geq 90\%$ rounded and smoothed surfaces (e.g., Fig. 2a); and (2) “broken” monzogranites, with $< 90\%$ rounded and smoothed surfaces (e.g., Fig. 3a).

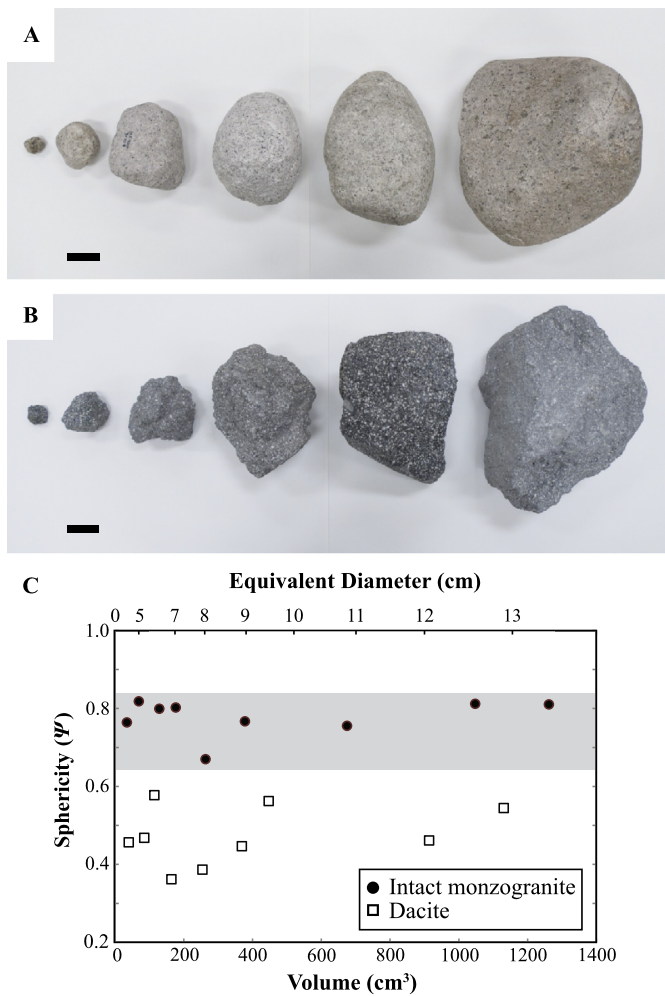


Fig. 2. Photographs of samples and sphericity data of accessory lithic clasts from the 2360 B.P. fallout deposits. (A) A selection of intact monzogranite clasts displaying the high degree of rounding and surface smoothness for a range of clast sizes (scale bar = 5 cm). (B) A similar size range of dacite clasts showing their subangular and relatively rough nature (scale bar = 5 cm). (C) Sphericity (Ψ) measurements determined by 3-D laser scanning of intact monzogranite (black circles) and dacite (open squares) clasts, plotted against clast volume. The shaded band highlights the consistently high sphericity values for the monzogranite lithics; dacite clasts have lower and more variable sphericity values. A two-tailed t -test shows the two suites to have different mean sphericities at the 95% confidence level.

3.3. Quantitative morphological analysis

Clast morphology comprises three main attributes: (i) form, which expresses dimensionality; (ii) roundness, which assesses the degree of angularity; and (iii) surface character, which summarizes overall smoothness and characteristic surface features (Barrett, 1980). Below, we define the metrics used to quantify the form, roundness and smoothness of individual clasts and, then, explore the covariations between clast sphericity, smoothness and size.

3.3.1. Sphericity

A sphere is the 3-D shape with the highest degree of roundness and the lowest ratio of surface area to volume. Our metric for clast sphericity (Ψ) uses measurements of clast volume (V) and surface area (S_A):

$$\Psi = \frac{36\pi V^2}{S_A^3} \quad (1)$$

Increasing values of Ψ denote increasing sphericity towards a perfect sphere ($\Psi = 1$; Fig. 2c). Surface area was measured by

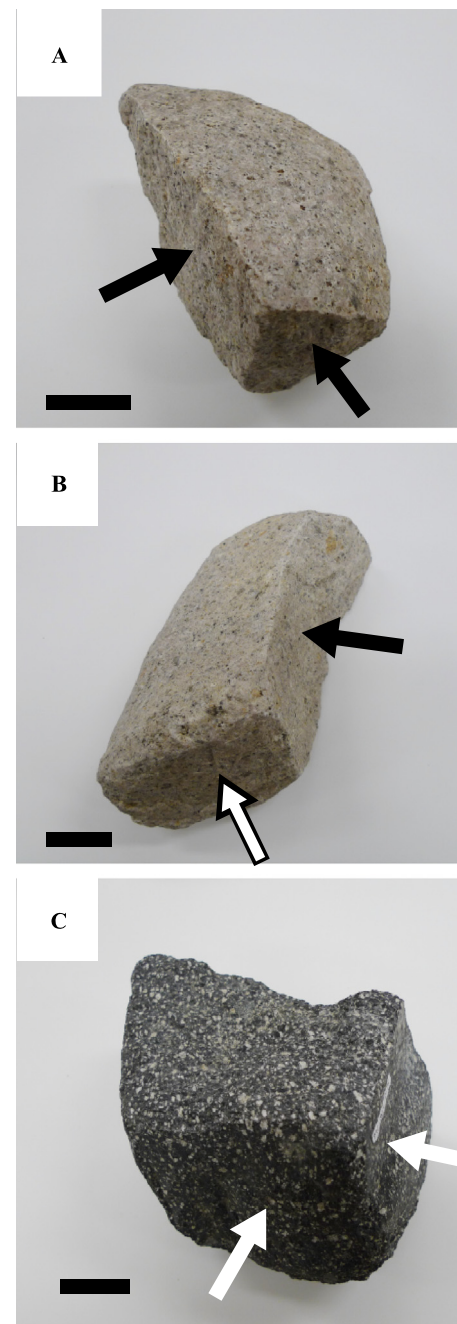


Fig. 3. Photographs of accessory lithic clasts recovered from the 2360 B.P. fallout deposits illustrating specific morphological features and structural relationships (scale bars = 5 cm). (A) Monzogranite clast featuring two clean fracture surfaces (black arrows) superimposed on an originally rounded clast. (B) Rounded monzogranite clast featuring late fracture surfaces that have edges recording different degrees of post-fracture rounding, indicating that the fractures occurred at different times during ascent. The face with subrounded edges (white arrow) is interpreted to represent a relatively early fracture surface of the clast, while the face with angular edges (black arrow) is interpreted to have formed during a later breakage event. (C) Dacite clast with clear primary columnar joint surfaces (white arrows) showing little attrition or smoothing.

scanning the exterior surface of each clast using a NextEngine™ 3-D laser scanner (e.g., Anochie-Boateng et al., 2011; Hayakawa and Oguchi, 2005). We applied this technique to a suite of 9 intact monzogranite and 9 dacite clasts ranging in size from 35 to 1262 cm³ (Fig. 2). The operational limits of the 3-D laser scanner limited the size range of the sample set. Monzogranite ($N = 7$) and dacite ($N = 7$) samples with volumes of <900 cm³ were scanned

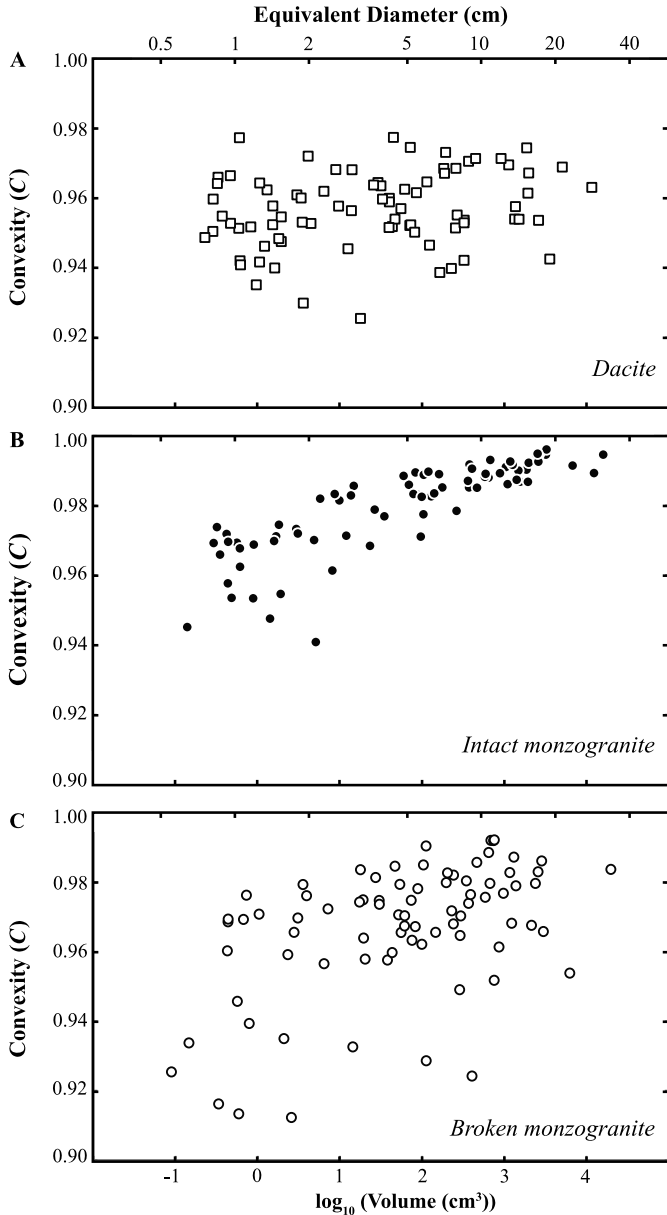


Fig. 4. Measured values of convexity (C) for accessory lithic clasts from image analysis of photographs for: (A) dacite lithic clasts; (B) intact monzogranite lithic clasts; and (C) broken monzogranite lithic clasts. Convexity results are plotted against measured clast volumes (lower axis) and the diameter of an equivalent sphere (upper axis). Statistical analysis of the convexity:volume trends shows a significant (p -value < 0.001) correlation for intact monzogranites ($r = 0.82$), a significant (p -value < 0.001) but relatively weak correlation for the broken monzogranites ($r = 0.47$), and a lack of significant (p -value = 0.078) correlation for the dacites ($r = 0.20$).

in ‘Macro’ mode at a resolution of $\sim 28,400$ points/cm². The larger (>900 cm³) samples were scanned in ‘Wide’ mode at a resolution of 7100 points/cm². The parameter ψ is sensitive to all three aspects of particle morphology: form, roundness, and overall smoothness. Thus, low sphericity values may indicate a highly elongate particle form, a highly angular, but equant, shape, or very rough and irregular particle surfaces (Fig. 2c).

3.3.2. Convexity

Surface roughness reflects the distribution and magnitude of the peaks (convexities) and depressions (concavities) on any object’s surface (e.g., Dinesh, 2008). We adopted particle convexity

(C) as a proxy for surface smoothness using 2-D cross-sectional images of individual clasts. Our metric for convexity is defined by:

$$C = \frac{A_{clast}}{A_{hull}} \quad (2)$$

where A_{clast} is the measured cross-sectional area of the clast and A_{hull} is the model convex hull area of the same clast (e.g., Beggan and Hamilton, 2010; Hamilton et al., 2011). A_{hull} is the area of the smallest convex polygon that can completely enclose the particle in question. High degrees of convexity (~ 1) correspond to smooth surfaces whilst rough surfaces will have decreasing values ($0 < C < 1$). C is a proxy for the smoothness of an object’s surface, provided that the object does not have large sections of continuous concavity.

Cross-sectional profiles of clasts were obtained via image analysis (cf. Manga et al., 2011). The clasts were aligned such that the shortest axes were vertical, photographed against a solid-colored background using a digital camera, converted to black and white in Adobe Photoshop®, and then analyzed in MATLAB® using a modified version of the script developed by Manga et al. (2011) to compute convexity values (Fig. 4).

3.3.3. Smoothness

We explored the smaller-scale surface smoothness of clasts using the NextEngine™ 3-D laser scanner (see Supplementary Appendix B). For each clast, we performed a high-resolution scan on a square patch of surface having the highest apparent smoothness (Supplementary Appendix B; Fig. B.1). Therefore, the resulting topographic maps are indicative of the maximum smoothness attained by each clast. We compare the relative surface smoothness of individual clasts using a dimensionless metric (S):

$$S = \frac{A_{proj}}{A_{meas}} \quad (3)$$

where A_{meas} is the 3-D surface area of the scanned patch and A_{proj} is the projected area of the square region (Fig. 5a). Values of S decrease from 1, a perfectly planar surface, as roughness increases. We collected smoothness data on a total of 20 monzogranite and 17 dacite clasts ranging in size from 15 to $\sim 12,000$ cm³ (Fig. 5b).

4. Results

The measured values of sphericity clearly differentiate the intact monzogranite clasts from dacite clasts of similar size (Fig. 2c). Monzogranite samples range from $0.67 \leq \psi \leq 0.82$ (mean $X_\psi = 0.78 \pm 0.05$) and dacite samples have values of $0.36 \leq \psi \leq 0.58$ ($X_\psi = 0.47 \pm 0.08$). Therefore, the monzogranite clasts are quantifiably, and significantly, more spherical than the dacite clasts.

The convexity values (C) obtained for dacite clasts range from $0.93 \leq C \leq 0.98$ (mean $X_C = 0.96 \pm 0.01$; Fig. 4a). In contrast, the intact monzogranite samples are demonstrably smoother based on a higher range and mean of convexity values ($0.94 \leq C \leq 1.0$; $X_C = 0.99 \pm 0.01$; Fig. 4b). Broken monzogranite clasts display the largest range of convexity values ($0.91 \leq C \leq 0.99$; $X_C = 0.97 \pm 0.02$; Fig. 4c). One of the major findings in this dataset is that convexity of the intact monzogranites is strongly and positively correlated to sample size (Fig. 4b). In other words, the extent of milling of the monzogranite clasts, as evidenced by smoothness, is positively correlated to size. The broken monzogranites show a weaker but clear positive correlation (Fig. 4c). Dacite clasts show no discernible correlation between surface smoothness and sample size (Fig. 4a vs. 4b, c).

Results of our 3-D laser scanner analysis for smoothness are summarized in Fig. 5b. Overall, the monzogranite suite is significantly smoother ($X_S = 0.96 \pm 0.03$) than the dacite sample set ($X_S = 0.86 \pm 0.03$). The smaller monzogranite clasts (<400 cm³)

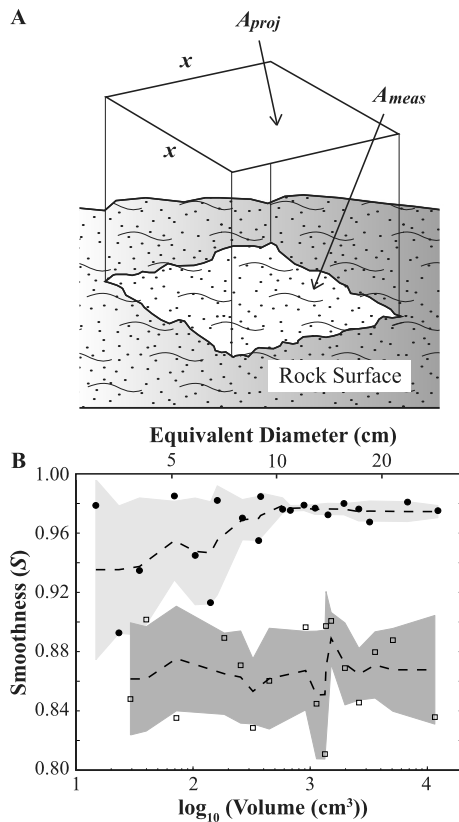


Fig. 5. Surface smoothness metric methodology and results. (A) Visual explanation of projected surface area (A_{proj}) and measured surface area (A_{meas}) used to compute smoothness (see text). (B) Smoothness of scanned surface regions for a selection of intact monzogranite (black circles) and dacite (open squares) lithic clasts, plotted against sample volume (lower axis) and volume equivalent diameter (upper axis). The moving average ($N = 3$) for each suite (dashed lines) and moving standard deviation (shaded fields) are used to accentuate the trend of increasing smoothness with clast size for the monzogranite clasts. The dacite samples show no correlation between clast size and smoothness.

show a large range in smoothness values ($0.89 \leq S \leq 0.98$). In contrast, larger monzogranite samples ($>400 \text{ cm}^3$) trend towards an increasingly narrow range of high smoothness values ($0.97 \leq S \leq 0.98$; Fig. 5b). The lower mean and higher variance of S values of the smaller monzogranites indicates that some of the smaller clasts remained rough while others achieved high levels of smoothness. The high mean and low variance in S values of the larger monzogranite accessory lithics indicates that they all attained high degrees of honing before being ejected. The dacites uniformly show significantly lower smoothness values ($0.81 \leq S \leq 0.90$) than their monzogranite counterparts. Of greater potential significance is the fact that the dacite accessory lithics show absolutely no correlation between sphericity, roundness, smoothness and sample size (Figs. 2b, 4, 5b). The 3-D surfaces of the dacite samples also typically display much greater relief and more surface irregularities than the intact monzogranite surfaces (e.g., Supplementary Appendix B, Fig. B.1).

5. Discussion

5.1. Milling processes

Two main types of processes operate on lithic clasts suspended in volcanic conduits during explosive eruptions: (i) mechanical processes driven by physical contact between the clast and other particles or wall rocks; and (ii) thermal processes, caused by the intense heat within the conduit.

Mechanical processes reshape clasts through attrition, whereby clasts continuously lose volume via a succession of breakages or surficial chipping caused by impacts with other solids (Durian et al., 2007). The energy of the particle–particle interaction strongly influences the resulting morphologies of the impacted clasts. In a numerical and experimental study of pumice clast attrition during conduit transport, Dufek et al. (2012) distinguished two types of clast collision. The first type involves high-energy impacts between two particles, or between particles and conduit walls, and causes the largest instantaneous reduction in clast volume ($\geq 25\%$). These impacts are termed “disruptive collisions” and have the potential for converting a single clast into multiple smaller fragments. The second type, termed “non-disruptive collisions,” involves low-energy collisions resulting in the loss of small volumes of material from the impacted clast. The abrasion of a rock via sandblasting is an example of gradual attrition through a multitude of non-disruptive collisions (Momber, 2004; Suzuki and Takahashi, 1981; Verhoef et al., 1984). The type of fragmentation resulting from a collision depends on the intrinsic properties of the particles (i.e. strength, grain size, homogeneity, texture, etc.) and the energy of the impact, which is, in turn, a function of the relative velocities and masses (i.e. sizes) of the clasts.

Evidence of both disruptive and non-disruptive collisions is clearly visible in the morphological characteristics of the monzogranite accessory lithic sample suite. Disruptive collisions are the best explanation for the relatively fresh fracture surfaces found on many of the larger accessory lithic clasts (e.g., “broken” monzogranite; Fig. 3a). Large-scale fracturing of homogeneous, strong, dense accessory lithic clasts (e.g., monzogranite or dacite) requires high-energy impacts typical of collisions with other dense objects, such as similar-sized lithic clasts or the conduit walls. On this basis, the majority of the fractured surfaces are taken as reflecting conduit processes rather than resulting from the impact attending their landing in the pumice fallout deposits.

Non-disruptive collisions are driven by the high-velocity interactions between the lithic fragments and the accelerating gas-pyroclast mixture filling the conduit above the fragmentation surface. These non-disruptive collisions are many orders of magnitude more frequent than disruptive events and cause continuous attrition and milling of the larger lithic clasts suspended in the gas jet. We term this process ash-blasting. Ash-blasting is similar in many respects to natural (e.g., aeolian) or industrial sandblasting (Kuenen, 1960; Suzuki and Takahashi, 1981) and is driven by high differential velocities between the upwards accelerating volcanic ash and the larger, denser lithic clasts. These high differential velocities cause the fragmented magma (e.g., ash-, lapilli-, block-sized juvenile pyroclasts) to behave as brittle, solid particles (i.e. glass) rather than as viscous melt (e.g., Dingwell and Webb, 1990). Lower differential velocities or lower melt viscosities would lead to melt coating of accessory lithic clasts as observed in explosive basaltic eruptions (e.g., Porritt et al., 2012) and less attrition. Most of the attrition of accessory lithics due to ash-blasting is confined to the volcanic conduit for two reasons. Firstly, the dusty gas jet in the conduit rapidly expands outward at the vent leading to a rapid drop in particle density and differential velocity, substantially reducing the abrasive potential of the eruptive column. Secondly, many of the large, dense lithics in this study were ejected from the vent as ballistics or were shed almost immediately from the lower portion of the eruption column (Fig. 1), thus rapidly bypassing the potentially abrasive eruption column.

Kuenen (1960) used a series of abrasion experiments to create a pictorial record of the gradual reshaping of cube-shaped clasts as a function of mass attrited (Fig. 6a). The cube-shaped samples continually lost mass, gradually becoming rounder until they attained a near perfect sphericity at $\sim 48\%$ mass loss (Fig. 6a). The shapes of the larger more rounded and smoothed clasts of monzogran-

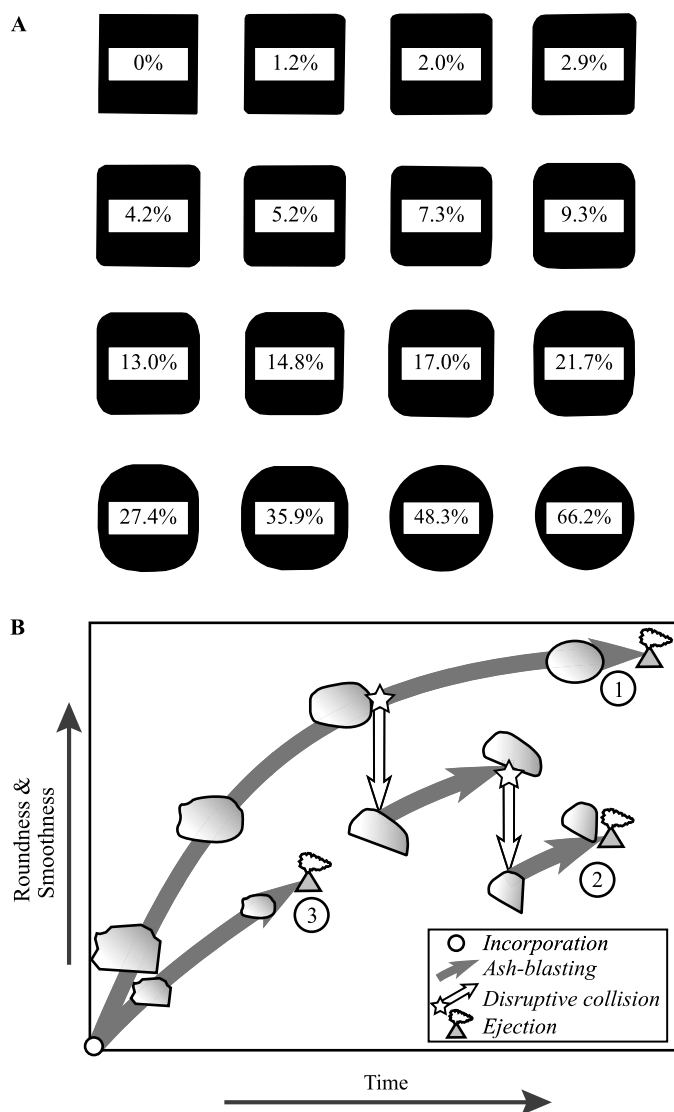


Fig. 6. Visual representation of progressive reshaping process of accessory lithic clasts within volcanic conduits. (A) Chart modified from [Kuenen \(1960\)](#) relates the degree of rounding of rock cubes to mass loss (%). (B) Schematic diagram relating roundness and smoothness of accessory lithic clasts to the conduit processes (ash-blasting, disruption) operating on the clasts and the residence time of the clast in the conduit prior to evacuation. Path #1: progressive reshaping of a deeply-sourced, large clast by ash-blasting and with no disruptive collisions (i.e. [Dufek et al., 2012](#)); the roundness and smoothness of the clast increases continuously while in the conduit until the clast is expelled. Path #2: clast is honed by ash-blasting but suffers two disruptive collisions during ascent; each collision causes immediate and substantial decreases in the clast's size affecting its residence time and reducing the clast's overall roundness and smoothness. Between disruptive events and evacuation the newly formed fracture surfaces continue to be honed by ash-blasting (cf. [Fig. 3b](#)). Path #3: small or shallowly sourced accessory clasts have substantially reduced residence times and, thus, less opportunity for reshaping. Small clasts also have lower terminal velocities, thereby, reducing the effectiveness of the ash-blasting process (see text).

ite (e.g., [Fig. 2a](#)) suggest ~30% or more mass loss assuming that failure of the conduit walls released initially blocky-shaped clasts ([Fig. 6a](#); [Kuenen, 1960](#)).

The broken monzogranite clasts record a more complicated history of disruptive collision events and concomitant rounding and smoothing by ash-blasting prior to being ejected ([Fig. 6b](#)). Following each disruptive collision, attrition by ash-blasting continues and the new fracture surfaces are immediately subject to renewed smoothing and rounding. Lithic clasts that have been subjected to multiple disruptive collisions can have several fracture surfaces

that show different degrees of honing (e.g., [Fig. 3b](#), [Fig. 6b](#)) reflecting the dynamic interplay between multiple clast-modifying processes.

Heating of lithic clasts has two potential effects. Firstly, the tensile strength (e.g., [Bauer and Johnson, 1979](#)), fracture toughness (e.g., [Atkinson et al., 1984](#); [Meredith and Atkinson, 1985](#)) and compressive strength (e.g., [Tullis and Yund, 1977](#)) of granitoids typically decrease substantially with increasing temperature. For example, [Bauer and Johnson \(1979\)](#) showed that the Brazilian tensile strength of the Westerly granite and the Charcoal granite decreased from ~13.5 MPa at 25 °C to only ~2 MPa when heated to 900 °C. Heating of conduit wall rocks and the entrained lithic clasts, therefore, increases the potential for lower energy collision events to cause disruption. Collisional events that would not be energetic enough to break off wall rocks or fragment large clasts at 25 °C may well cause failure at conduit temperatures. Surface erosion by sandblasting is the product of compressive failure during impact and tensile failure during elastic rebound ([Verhoef et al., 1984](#)). Thus, heating of clasts can also increase the efficiency of the non-disruptive comminution or attrition of lithic clasts by ash-blasting processes.

Secondly, and perhaps more importantly, rapid heating of clasts can cause differential thermal expansion of the clast rim versus its interior, producing tangential compression within the rim and radial tension in the core ([Preston and White, 1934](#)). These stresses are partially released by thermal spalling manifest by explosive flaking of the clast's surface (i.e. spalls; [Preston and White, 1934](#); [Thirumalai, 1969](#)). Evidence of thermal spalling is present in many monzogranite clasts in the form of thin, concentric, partially detached spalls present on their surfaces. These partial spalls would be easily removed via ash-blasting thereby enhancing the overall rates of attrition.

5.2. Conduit diameter estimation

Accessory lithic clasts mainly originate from erosion of conduit wall rocks when they fail under tension caused by pressure fluctuations in the conduit (i.e. if $P_{lithostatic} > P_{conduit}$) ([Macedonio et al., 1994](#); [Mitchell, 2005](#); [Varekamp, 1993](#); [Wilson et al., 1980](#)). Once entrained into the particle-laden stream of expanding gas, the clasts may be lofted upwards, sink, or find a level of neutral buoyancy depending on their mass and the ambient properties of the eruptive flux. The absolute velocity of the clast relative to the surface (U_R) is modeled as:

$$U_R = U_G - U_T \quad (4)$$

where U_G is the velocity of the dusty gas jet, and U_T is the differential velocity between the clast and the dusty gas. We adopt the formulations of [Wilson et al. \(1980\)](#) and [Parfitt and Wilson \(2008\)](#) for the estimation of U_T and U_G within the volcanic conduit. Above the fragmentation front and at high Reynolds numbers, U_T is modeled, for spherical clasts of diameter (d) and density (ρ_c), as:

$$U_T = \sqrt{\frac{4dg(\rho_c - \rho_g)}{3C_D\rho_g}} \quad (5)$$

where ρ_g is the density of the gas phase, g is gravitational acceleration, and C_D is a drag coefficient appropriate for large, smooth particles entrained in the volcanic conduit at high Reynolds numbers ($C_D = 1.2$; Supplementary Appendix C) ([Walker et al., 1971](#); [Wilson et al., 1980](#)). This simple drag coefficient estimate is applied uniformly to all lithics in our model, without accounting for potential variations in the drag coefficient caused by slight changes in Reynolds number within the conduit, or drag forces imparted through collisions with smaller particles (i.e. the ash-laden jet)

(e.g., Dufek et al., 2009). Gas velocities (U_G) within a cylindrical conduit are modeled as:

$$U_G = \frac{4M_f}{\pi\rho_B D^2} \quad (6)$$

where M_f is the mass flux of the eruption, ρ_B is the bulk density of the particle–gas mixture, and D is the diameter of the volcanic conduit (Parfitt and Wilson, 2008; Wilson et al., 1980). Values of M_f can be estimated from the heights of sustained eruption columns:

$$H = 0.236\sqrt[4]{M_f} \quad (7)$$

(Wilson et al., 1980). Bulk density (ρ_B) is dictated by the exsolved weight fraction of gas (n_f) and the melt density (ρ_m) (Supplementary Appendix C; Wilson et al., 1980):

$$\frac{1}{\rho_B} = \frac{n_f}{\rho_g} + \frac{(1-n_f)}{\rho_m} \quad (8)$$

The bulk density of the expanding ash–gas mixture within the conduit (ρ_B) changes with depth due to decreasing pressure (P) as described by:

$$\rho_g = \frac{P \cdot m}{R \cdot T} \quad (9)$$

where m and T are the molar weight and temperature of the gas phase, respectively, and R is the universal gas constant (Supplementary Appendix C; Parfitt and Wilson, 2008).

We have adopted a value of 16 km for the column height of the 2360 B.P. subplinian eruption (cf. 15–17 km; Hickson et al., 1999; Luty, 1994) which suggests a mass flux (M_f) of 2.1×10^7 kg/s (Eq. (7); Supplementary Appendix C). Using Eq. (4) and Eq. (9) we have calculated model velocities for clasts within the conduit as a function of depth and for conduit diameters of 20, 40 and 60 m (cf. Supplementary Appendix C; Fig. 7). The calculations show how gas velocity (U_G), and, thus, the relative velocities of lithic clasts (U_R), increase upwards due to gas expansion (Fig. 7). For a fixed mass flux (M_f), the velocity profiles change greatly as a function of conduit diameter (Fig. 7a, b, c); smaller conduits generate higher gas velocities and will impart higher lofting velocities to lithic clasts (Fig. 7a). A 20 m diameter conduit lifts 50 cm diameter lithic clasts at 30 ms^{-1} at 2 km depths. At similar depths, the same sized clasts in a 60 m diameter conduit are non-eruptible.

There have been a number of approaches taken to estimate the diameters of volcanic conduits in the subsurface (e.g., Melnik and Sparks, 2006; Melnik et al., 2011; Papale and Dobran, 1993). Here, we use the largest monzogranite clast recovered from the proximal fallout deposits to constrain the conduit diameter. The clast is highly rounded, weighs 51.7 kg, has orthogonal dimensions of $44.7 \times 34.9 \times 28.6$ cm, and has a volume of $20 \times 10^3 \text{ cm}^3$ (equivalent spherical diameter of ~ 34 cm). Based on the size of this clast, the apparent absence of substantially larger lithic clasts, and the minimum source depth of monzogranite clasts (i.e. 700 m, Fig. 1), the conduit for the 2360 B.P. eruption is likely to have been ~ 40 – 45 m in diameter (Fig. 7). This accords well with the sizes of conduits established for subplinian to plinian eruptions (10–100 m) and the range (20–60 m) expected for an eruption with $M_f = 2.1 \pm 10^7$ kg/s (Wilson et al., 1980). In our approach, depth to the source rock is a critical constraint because the capacity of the expanding dusty gas jet to loft lithics increases nonlinearly with decreasing depth. Below we assume the conduit diameter for the 2360 B.P. eruption is 42 m to allow for eruption of deeper-sourced monzogranite lithic clasts up to 40 cm in diameter.

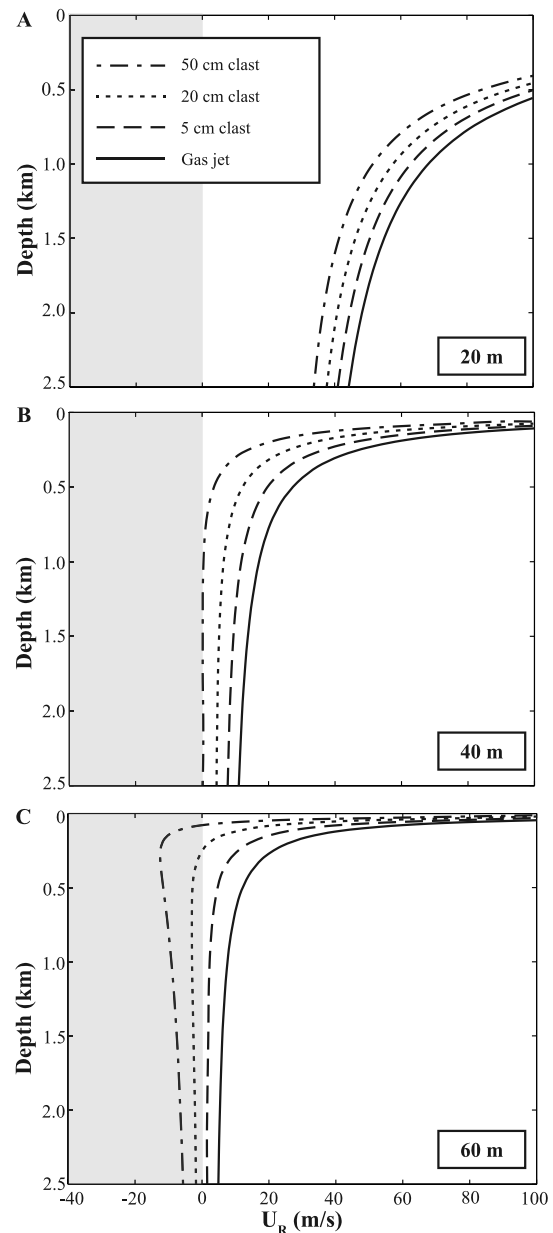


Fig. 7. Relative velocity (U_R) profiles of lithic clasts within model volcanic conduit (see text). U_R profiles show velocity relative to a fixed reference frame as a function of depth in conduit, including the velocity of the conduit-filling dusty gas jet, and the velocities of 5 cm, 20 cm, and 50 cm accessory lithic clasts. All clasts are assumed to be spherical and have a density of 2590 kg/m^3 . U_R profiles are computed for conduit diameters of: (A) 20 m; (B) 40 m; and (C) 60 m. Increasing conduit diameter causes a marked decrease in U_R ; shaded zones in each panel denote conditions for negative velocities (i.e. clast sinking vs. clast lofting).

5.3. Residence times

The morphological properties of the accessory lithic clasts showed that: (1) dacites are rougher and less rounded than monzogranites (Fig. 2); and (2) large monzogranites are smoother than small monzogranites (Figs. 4, 5b). Below, we present a model to explain these two observations on the basis of differential ash-blasting velocities and the minimum residence times of individual clasts.

We have used the model velocity–depth relationships for individual clasts (cf. Fig. 7) to compute clast residence times within the 2360 B.P. conduit. Residence time (t_R) is the time taken by the clast to move from source to the surface (Fig. 8). Values of t_R are

calculated by numerically integrating the velocity-depth curves of individual clasts of different sizes (cf. Fig. 7). This yields a minimum residence time assuming one-way lofting with no cycling (Fig. 8). Values of t_R depend on clast density, size, and depth of incorporation.

Small lithic clasts have short residence times (<4 min for a 2 cm clast; Fig. 8a) because they have low terminal velocities and are nearly coupled to the dusty gas stream. Larger clasts will have correspondingly greater residence times (up to ~8 min for a 20 cm clast; Fig. 8b). However, source depth also controls clast residence times (dashed lines in Fig. 8b, c), and clasts sourced from shallower depths will have substantially shorter residence times (Fig. 8c). For example, while a 30 cm lithic sampled at depths of 2.5 km resides in the conduit for ~15 min, an equivalent clast incorporated at 0.5 km depth is evacuated in ~1 min (Fig. 8c).

Our model can also explain the strong positive correlation between clast size and degree of smoothing exhibited by the monzogranite clasts and absent in dacite clasts (Figs. 4, 5b). Isochron contour maps of source time as a function of clast diameter and source depth (Fig. 9) display 3 broad fields: (i) a field of non-eruptible conditions where the clast size or source depth preclude lofting; (ii) a field where $t_R < 0.5$ min regardless of clast size, and (iii) a field contoured for t_R that supports clast evacuation. Increasing conduit diameter (Fig. 9) expands the non-eruptible field by reducing the maximum size of loftable lithics (cf. Fig. 7) and increases the overall residence times of eruptible lithic clasts. Vertical traverses across the contoured field show the decrease in residence time for similar sized clasts with decreasing sample depth. Horizontal traverses show the increase in t_R with increasing clast size until the non-eruptible field is reached. Fig. 9, therefore, offers an explanation for the observed variations in degree of milling of accessory lithic clasts. Because of their shallow source, dacite clasts (<550 m; Fig. 1) will have residence times of <2 min regardless of size, allowing for little variation in the extent of milling. In contrast, the residence times of the deeper-seated monzogranite lithics (>700 m; Fig. 1) can vary substantially (from ~1 minute to over an hour; Fig. 9) depending on clast size and depth of sampling. Thus, the extent of milling (rounding and surface honing) varies and increases substantially with increasing clast size and increasing sample depth.

5.4. Rates of attrition

How rapidly does thermomechanical milling of accessory lithic clasts operate? We have modeled the rates of attrition for the *ash-blasting* process by combining the model residence times for a 42 m conduit (Fig. 9b) with estimates of mass lost for the rounded lithics (Fig. 6a). The general description for total volume loss of a milled clast (ΔV) is given by:

$$\Delta V = V_o - V_f \quad (10)$$

where V_o and V_f are the original volume and final volume of the clast, respectively. The attrition rate (R) of an abraded clast is then given by:

$$R = \frac{\Delta V}{t_R} \quad (11)$$

where t_R is the residence time of the clast. Finally, the initial and final volumes of an attrited clast can be described by:

$$V_f = (1 - f)V_o \quad (12)$$

where f is the fraction of mass lost (e.g., Kuenen, 1960; Fig. 6a).

For constant conduit conditions (e.g., mass flux, conduit diameter, etc.), R depends mainly on: (i) residence time, (ii) surface area available for ash-blasting, and (iii) the effective or differential

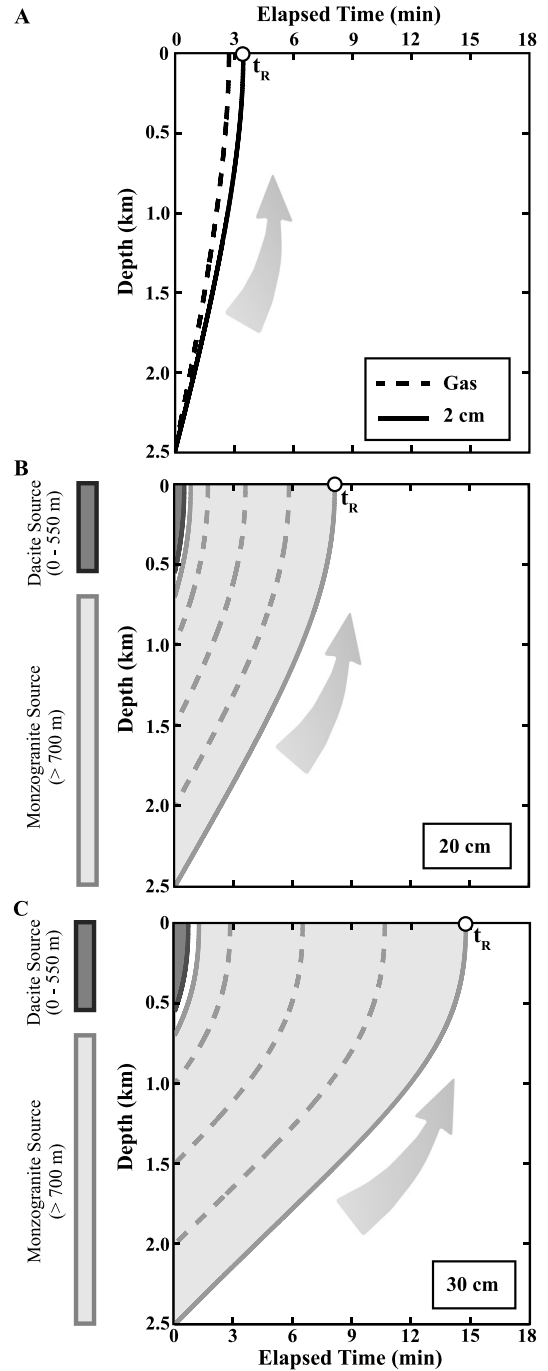


Fig. 8. Transit times for accessory lithic clasts lofted within a 42 m diameter conduit to the point of ejection, as a function of entrainment depth (e.g., wall rock source depth). Residence times are shown for clast diameters of: (A) 2 cm, (B) 20 cm, and (C) 30 cm. The lowermost solid line in each panel shows the cumulative time a clast sourced at 2500 m spends in the conduit prior to eruption: t_R denotes the total residence time. Dashed lines are timelines for clasts originating from depths of 2, 1.5, and 1 km. The pale gray shading encloses ascent timelines for monzogranite lithics sourced between 700 m and 2.5 km. The dark gray shading encloses ascent timelines for the shallow-sourced (0–550 m) dacite lithic clasts. In a 42 m diameter conduit the residence times for a 30 cm clast vary between 16 min for monzogranite sourced from 2.5 km vs. ~1 min for dacite from a wall rock depth of 550 m.

impact velocity (Momber, 2004; Suzuki and Takahashi, 1981). The impact velocity (e.g., *ash-blasting* velocity) is taken here as the velocity of the ash-laden stream relative to the lithic (e.g., U_T). Thus, larger lithic clasts, having larger terminal velocities, are subject to higher ash-blasting velocities, and will feature higher rates of at-

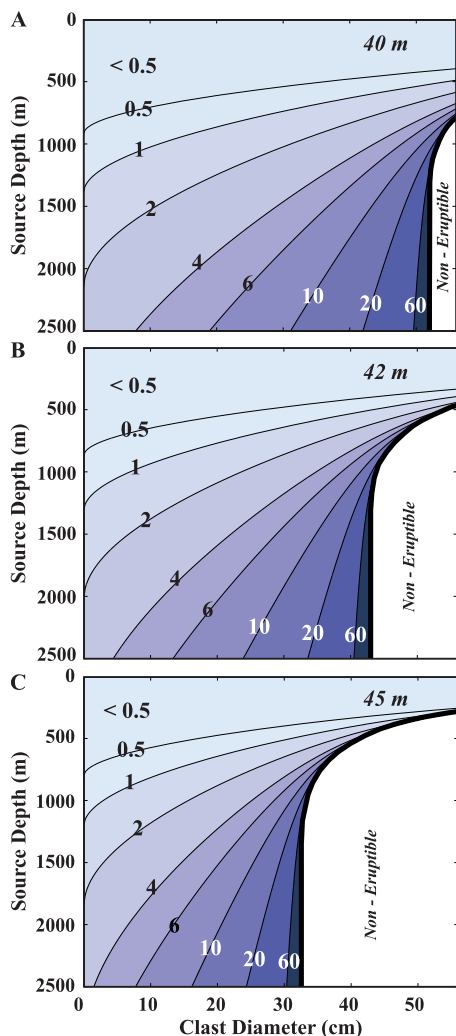


Fig. 9. Contour plots of residence time (min) of accessory lithic clasts within the volcanic conduit as a function of clast size (x-axis) and source depth (y-axis). The heavy black line denotes “infinite” residence time where a clast has zero velocity at a specific depth; larger clasts are not lofted and fall within the “non-eruptible” zone. Contour plots are for conduit diameters of: (A) 40 m diameter; (B) 42 m diameter; and (C) 45 m diameter. The size and the source depth of lithic clasts, as well as the conduit diameter, all exert a notable influence on clast residence time. Conduit diameter also exerts a strong control on the size of the maximum lithic clast eruptible from a given source depth.

trition. Smaller clasts, having low terminal settling velocities, will have lower attrition rates. Sandblasting studies suggest that attrition rate (R) is proportional to the kinetic energy (E_k) and, thus, the square of impact velocity (i.e. U_T):

$$R \propto E_k \propto U_T^2 \quad (13)$$

(Suzuki and Takahashi, 1981). We have used the clast’s weighted mean terminal velocity (U_T^{mean}) on its path from source to depth (Fig. 7; $U_R - U_G$) as the effective ash-blasting velocity. Assuming that attrition rate is proportional to the surface area (S_A) suggests the following relationship:

$$\frac{dV}{dt} = \xi \cdot S_A \cdot (U_T^{mean})^2 \quad (14)$$

where ξ is a normalized attrition rate coefficient, to be determined empirically, and having units of s m^{-1} . Integration of Eq. (14) across the volume limits expressed in Eq. (12) yields a relationship between the fractional mass loss (f), final particle radius (r_f), differential velocity, and residence time (t_R) (see derivation in Supplementary Appendix D):

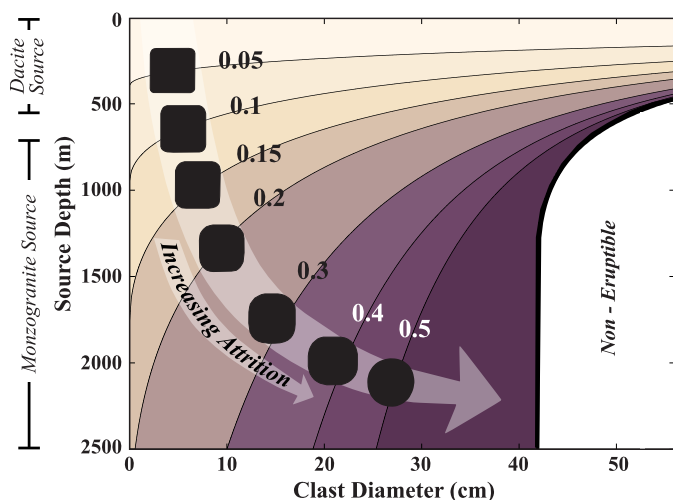


Fig. 10. Contour plot of f values (% mass loss; see text) of accessory lithic clasts within a 42 m diameter conduit, as a function of final clast size (x-axis) and source depth (y-axis). The silhouettes of experimentally rounded clasts (Kuenen, 1960), are positioned on the appropriate % mass loss contours (see Fig. 7a), thereby, emphasizing the amount of attrition due to volcanic ash-blasting required to create rounded accessory lithic clasts. The amount of attrition and, thus, the extent of rounding is strongly controlled by both the size and source depth of the lithic clasts.

$$f = 1 - \left(\frac{r_f}{r_f - \xi \cdot (U_T^{mean})^2 \cdot t_R} \right)^3 \quad (15)$$

We have calibrated the attrition rate model (Eq. (15)) by obtaining a value of ξ using observations on the monzogranite lithic clasts. Monzogranite lithics >10 cm in diameter show the maximum amounts of clast smoothing or honing (Fig. 5b). Based on the Kuenen (1960) diagram (Fig. 6a), the roundest 10 cm monzogranite clasts in the collection suggest $\sim 30\%$ mass lost ($f = 0.3$). For a 10 cm diameter lithic, sourced from a maximum depth of ~ 2500 m, we obtain a mean differential velocity (U_T^{mean}) value of 6.6 m s^{-1} and a residence time (t_R) of 315 s. These values imply (Eq. (15)) a minimum value for the attrition rate coefficient (ξ) of $-4.57 \times 10^{-7} \text{ s m}^{-1}$. Assuming a source depth shallower than 2500 m would yield higher absolute values of ξ , ascribing a higher efficiency to the ash-blasting process. An attrition rate coefficient was not specifically computed for the dacite clasts, as most of these clasts display very little attrition (i.e. $f \pm 0$). However, we expect the ash-blasting attrition rate of the competent dacite clasts to resemble that of the monzogranite clasts.

We have used this empirical value of ξ to convert our contoured values of clast residence times (Fig. 9) into a plot contoured for the fraction of material (f) removed via ash-blasting (Fig. 10). As expected, very shallow-sourced lithics will display a relatively narrow range of mass loss fractions (e.g., $<5\%$ mass loss for lithics sourced <200 m) regardless of clast size, while deeper-sourced lithics display a wide range of mass loss fractions depending on the clast size (Fig. 10). This dependence of total attrition on source depth further explains the uniformly high degree of angularity of the dacite lithic sample set. For example, dacite lithics up to 25 cm in diameter will undergo $<12\%$ total attrition (Fig. 10). Highly rounded dacite accessory lithics could only be produced if very large (>40 cm diameter) dacite clasts are incorporated at the lowest possible reaches of the dacite source body (i.e. 450–550 m depth). The lack of any very large and highly milled dacite clasts in the proximal PCF fallout deposits precludes this possibility, an indication that the largest dacite clasts were sourced at relatively shallow depths.

Fig. 10 shows that monzogranite clasts may display a wide range of f values, ranging from 0.07 to >0.5 , depending on their size and source depth. It should also be noted that the maximum

f value considered here is 0.5, as clasts achieve maximal rounding at approximately this level of attrition (Kuenen, 1960). As attrition progresses beyond this point, clasts will continue to shrink in size, but cannot become more rounded (Fig. 6a). Small monzogranite lithics (<5 cm diameter) can display a wide range of f values, ranging from 0.08 to 0.25 depending on source depth (Fig. 10). This wide range in f values provides an explanation for the diverse smoothness values obtained for the <5 cm monzogranite clasts (Figs. 4b, 5b).

We have used Eq. (11) to compute the total rates of attrition (R) by ash-blasting for lithic clasts of different sizes but deriving from the same depth (2500 m). Each clast has a different model f values due to differences in their residence times and differential velocities (Fig. 10). The volumetric attrition rates for 2, 10, and 25 cm diameter clasts ($\text{cm}^3 \text{s}^{-1}$) are computed using the model value of ξ (attrition rate coefficient) determined above; the values vary by 4 orders of magnitude: 6×10^{-3} , 7×10^{-1} , and $12 \text{ cm}^3 \text{ s}^{-1}$, respectively. The corresponding rates of reduction in clast radius are: 4×10^{-4} , 2×10^{-3} , and $6 \times 10^{-3} \text{ cm s}^{-1}$.

Volcanic ash-blasting most closely approximates industrial sandblasting where concrete or rock surfaces are bombarded by a stream of small abrasion projectiles (i.e. quartz grains; Suzuki and Takahashi, 1981; Verhoef et al., 1984). Sandblasting projectile velocities are on the order of 10 to 150 m/s, and particle mass fluxes are on the order of 2 to $5 \text{ g s}^{-1} \text{ cm}^{-2}$. Typical sandblasting abrasion rates for strong, dense, competent materials span a range of values (8×10^{-5} to $3 \times 10^{-4} \text{ cm s}^{-1}$) depending on the target properties (Momber, 2004; Suzuki and Takahashi, 1981). Our model calculations for ash-blasting suggest a range of velocities (1 to 200 m s^{-1} ; Eq. (5)) overlapping sandblasting velocities. However, we predict several orders of magnitude higher attrition rates for volcanic ash-blasting (4×10^{-4} to $6 \times 10^{-3} \text{ cm s}^{-1}$ for 2 to 25 cm diameter clasts). We suggest that the main reason for the orders of magnitude higher attrition rates attending explosive eruptions is the exceedingly high particle densities in the expanding gas jet (relative to sandblasting operations). Within the 42 m diameter conduit to the 2360 B.P. eruption of Mount Meager, the particle mass flux was $\sim 1500 \text{ g s}^{-1} \text{ cm}^2$ – approximately 3 orders of magnitude larger than in commercial sandblasting jets (e.g., Suzuki and Takahashi, 1981).

5.5. Further implications for volcanic milling

Our study highlights the wealth of information that can be gained from accessory lithic clasts and some of the implications of the presence of milled lithic clasts within pyroclastic deposits. Rounded accessory lithics have been described in diverse volcanic deposits, ranging from scoria cone deposits (e.g., Francis and Oppenheimer, 2003; Franz et al., 1997) to the lag breccias within ignimbrite sheets (e.g., Allen and Cas, 1998; Mellors and Sparks, 1991; Nairn et al., 1994). The lag breccia deposits comprise mainly coarse, dense material that is simply too heavy to be transported far from the source in pyroclastic density currents. These short transport distances severely limit the amount of post-eruption comminution that these lithics experience. Interestingly, Allen and Cas (1998) and Nairn et al. (1994) also noted that the larger lithic clasts tended to be the roundest. The milling of accessory lithics in pyroclastic deposits has commonly been ascribed to ball-milling in the vent, or repeated ejection and fallback into the vent (Francis and Oppenheimer, 2003; Franz et al., 1997; Nairn et al., 1994). In contrast, our model views the milling and honing of accessory lithics as a process operating within the volcanic conduit that progressively modifies clasts during their ascent. Furthermore, volcanic ash-blasting should also affect juvenile clasts within the conduit.

The formation of a highly rounded (albeit not perfectly spherical) clast from an initially blocky form requires $\sim 30\%$ mass loss (Fig. 6a). Highly rounded and smoothed lithic clasts ($f > 0.3$; Fig. 10) form under a restricted range of conditions (e.g., clast size, source depth). Thus, the presence of highly rounded lithics in pyroclastic deposits has important implications for conduit geology, properties, and processes. Conversely, the eruption of angular ($f < 0.05$) rough lithics necessitates very little lithic attrition via ash-blasting, and also constrains aspects of the explosive eruption. For example, low degrees of lithic attrition may be due to relatively shallow lithic source depths or to relatively high gas jet velocities reflecting a high mass flux or a narrower conduit (Eq. (6)). Estimates of total mass attrition combined with knowledge of clast source depths provide an alternate means to constrain eruption mass flux rates, conduit diameters, or conduit gas jet velocities.

We further postulate that the degree of rounding and honing of lithic clasts can also be used to place constraints on the fragmentation depth of volcanic eruptions. Notably, an abundance of highly angular lithics may be indicative of a shallow fragmentation front, whereby the lithics all had short distances to travel before exiting the conduit, resulting in short residence times that precluded any significant rounding or honing. This represents an alternative means of monitoring the depth of the fragmentation front in conduits where the wall rocks are lithologically homogeneous.

6. Conclusions

Accessory lithic clasts are an important component of pyroclastic deposits that, to date, have been largely underutilized in volcanological studies. Here, we have presented the first detailed study of accessory lithic morphology. Milling of lithic clasts involves contributions from three main processes: disruptive fragmentation, ash-blasting, and thermal effects. We have presented a model that provides an understanding of these milling processes and ultimately relates clast morphology and surface properties to residence times in volcanic conduits. In addition, we have outlined a new method of estimating conduit diameter, by combining knowledge of the subsurface below the vent with maximum lithic size distributions. The final degree of rounding observed in accessory lithic clasts is primarily a function of the size and source depth of the lithic clast. The efficiency of high particle density ash-blasting within the conduit is enhanced by the heating of the lithic clasts to conduit-temperatures causing thermal weakening and increasing the rates of attrition. Indeed, volcanic ash-blasting may be the most efficient rock milling process in nature.

Acknowledgements

JKR is supported by the Natural Sciences and Engineering Research Council of Canada via the Discovery Grants program. LP is funded by a Marie Curie Research Fellowship. MEC was partially supported by a scholarship from the Fonds Québécois de Recherche sur la Nature et les Technologies. We gratefully acknowledge In-nergex Renewable Energy Inc. for allowing us access to their diamond drill core from the Mount Meager area. Our research on this topic was stimulated by conversations with Ray Cas and Hugh Tuffen. We thank Michael Manga and one anonymous reviewer for their constructive comments which have served to improve the clarity of the manuscript.

Appendix A. Supplementary material

Supplementary material related to this article can be found online at <http://dx.doi.org/10.1016/j.epsl.2013.07.008>.

References

- Allen, S.R., Cas, R.A.F., 1998. Lateral variations within coarse co-ignimbrite lithic breccias of the Kos Plateau Tuff, Greece. *Bull. Volcanol.* 59, 356–377.
- Andrews, G.D.M., Russell, J.K., Stewart, M.L., in preparation. The rise and fall of a welded pyroclastic dam: the 2,360 BP eruption of Mount Meager, British Columbia, Canada. *Bull. Volcanol.*
- Anochie-Boateng, J.K., Komba, J.J., Mvelase, G.M., 2011. Advanced and automated laser-based technique to evaluate aggregates. In: IRF International Road Congress – Innovations in Road Infrastructure. Moscow, Russia, 22–24 November, 2011, p. 11.
- Atkinson, B.K., MacDonald, D., Meredith, P.G., 1984. Acoustic response and fracture mechanics of granite subjected to thermal and stress cycling experiments. In: Hardy, H.R., Leighton, F.W. (Eds.), *Proceedings of the 3rd International Conference on Acoustic Emission/Microseismic Activity in Geological Structures and Materials*. Trans-Tech Publications, Clausthal, Germany, pp. 5–18.
- Barrett, P.J., 1980. The shape of rock particles, a critical review. *Sedimentology* 27, 291–303.
- Bauer, S.J., Johnson, B., 1979. Effects of slow uniform heating on the physical properties of the Westerly and Charcoal granites. In: 20th U.S. Symposium on Rock Mechanics. Austin, Texas.
- Beggan, C., Hamilton, C.W., 2010. New image processing software for analyzing object size-frequency distributions, geometry, orientation, and spatial distribution. *Comput. Geosci.* 36, 539–549.
- Campbell, M., 2012. Thermomechanical milling of lithics in volcanic conduits. MSc Thesis. University of British Columbia, Vancouver, B.C. p. 202.
- Clague, J.J., Evans, S.G., Rampton, V.N., Woodsworth, G.J., 1995. Improved age estimates for the White River and Bridge River tephra, western Canada. *Can. J. Earth Sci.* 32, 1172–1179.
- Dinesh, S., 2008. Computation of surface roughness of mountains extracted from Digital Elevation Models. *J. Appl. Sci.* 8, 262–270.
- Dingwell, D.B., Webb, S.L., 1990. Relaxation in silicate melts. *Eur. J. Mineral.* 4, 427–449.
- Dufek, J., Manga, M., Patel, A., 2012. Granular disruption during explosive volcanic eruptions. *Nat. Geosci.* 5, 561–564.
- Dufek, J., Wexler, J., Manga, M., 2009. Transport capacity of pyroclastic density currents: Experiments and models of substrate-flow interaction. *J. Geophys. Res.* 114, 1–13.
- Durian, D.J., Bideaud, H., Düringer, P., Schroder, A.P., Marques, C.M., 2007. Shape and erosion of pebbles. *Phys. Rev. E* 75, 1–9.
- Francis, P., Oppenheimer, C., 2003. *Volcanoes*, 2nd ed. Oxford University Press.
- Franz, G., Breikreuz, C., Coyle, D.A., El Hur, B., Heinrich, W., Paulick, H., Pudlo, D., Smith, R., Steiner, G., 1997. The alkaline Meidob volcanic field (Late Cenozoic, northwest Sudan). *J. Afr. Earth Sci.* 25, 263–291.
- Green, N.L., Armstrong, R.L., Harakal, J.E., Souther, J.G., Read, P.B., 1988. Eruptive history and K–Ar geochronology of the Late Cenozoic-Garibaldi Volcanic Belt, southwestern British Columbia. *Geol. Soc. Am. Bull.* 100, 563–579.
- Hamilton, C.W., Fagents, S.A., Thordarson, T., 2011. Lava-ground ice interactions in Elysium Planitia, Mars: Geomorphological and geospatial analysis of the Tartarus Colles cone groups. *J. Geophys. Res.* 116, 1–26.
- Hayakawa, Y., Oguchi, T., 2005. Evaluation of gravel sphericity and roundness based on surface-area measurement with a laser scanner. *Comput. Geosci.* 31, 735–741.
- Hickson, C.J., Russell, J.K., Stasiuk, M.V., 1999. Volcanology of the 2350 B.P. eruption of Mount Meager Volcanic Complex, British Columbia, Canada: Implications for hazards from eruptions in topographically complex terrain. *Bull. Volcanol.* 60, 489–507.
- Hutchison, C.S., 1974. *Laboratory Handbook of Petrographic Techniques*. John Wiley & Sons.
- Kuenen, P.H., 1960. Experimental abrasion 4: Eolian action. *J. Geol.* 68, 427–449.
- Luty, J.R., 1994. Eruption Characteristics and Industrial Application Potential of the Bridge River Airfall Pumice Deposit, Mount Meager, Southwestern British Columbia. University of British Columbia, Vancouver, B.C., p. 41.
- Macedonio, G., Dobran, F., Neri, A., 1994. Erosion processes in volcanic conduits and application to the AD 79 eruption of Vesuvius. *Earth Planet. Sci. Lett.* 121, 137–152.
- Manga, M., Patel, A., Dufek, J., 2011. Rounding of pumice clasts during transport: field measurements and laboratory studies. *Bull. Volcanol.* 73, 321–333.
- Mellors, R.A., Sparks, R.S.J., 1991. Spatter-rich pyroclastic flow deposits on Santorini, Greece. *Bull. Volcanol.* 53, 327–342.
- Melnik, O., Sparks, S., 2006. Transient models of conduit flows during volcanic eruptions. In: Mader, H.M., Coles, S.G., Connor, C.B., Connor, L.J. (Eds.), *Statistics in Volcanology*. Geological Society of London, pp. 201–213.
- Melnik, O.E., Blundy, J.D., Rust, A.C., Muir, D.D., 2011. Subvolcanic plumbing systems imaged through crystal distributions. *Geology* 39, 403–406.
- Meredith, P.G., Atkinson, B.K., 1985. Fracture toughness and subcritical crack growth during high-temperature tensile deformation of Westerly granite and Black gabbro. *Phys. Earth Planet. Inter.* 39, 33–51.
- Michol, K.A., Russell, J.K., Andrews, G.D.M., 2008. Welded block and ash flow deposits from Mount Meager, British Columbia, Canada. *J. Volcanol. Geotherm. Res.* 169, 121–144.
- Mitchell, K.L., 2005. Coupled conduit flow and shape in explosive volcanic eruptions. *J. Volcanol. Geotherm. Res.* 143, 187–203.
- Momber, A.W., 2004. Damage to rocks and cementitious materials from solid impact. *Rock Mech. Rock Eng.* 37, 57–82.
- Nairn, I.A., Wood, C.P., Bailey, R.A., 1994. The Reporoa Caldera, Taupo Volcanic Zone: source of the Kaingaroa Ignimbrites. *Bull. Volcanol.* 56, 529–537.
- Nasmith, H., Mathews, W.H., Rouse, G.E., 1967. Bridge River ash and some other recent ash beds in British Columbia. *Can. J. Earth Sci.* 4, 163–170.
- Papale, P., Dobran, F., 1993. Modeling of the ascent of magma during the plinian eruption of Vesuvius in A.D. 79. *J. Volcanol. Geotherm. Res.* 58, 101–132.
- Parfitt, E.A., Wilson, L., 2008. *Fundamentals of Physical Volcanology*. Blackwell Publishing, Oxford.
- Porritt, L.A., Russell, J.K., Quane, S.L., 2012. Pele's tears and spheres: Examples from Kilauea Iki. *Earth Planet. Sci. Lett.* 333–334, 171–180.
- Preston, F.W., White, H.E., 1934. Observations on spalling. *J. Am. Ceram. Soc.* 17, 137–144.
- Read, P.B., 1977a. Meager Creek volcanic complex, southwestern British Columbia. Report of Activities, Part A. *Geol. Surv. Can. Paper* 77–1A, pp. 277–281.
- Read, P.B., 1977b. Geology of Meager Creek geothermal area, British Columbia. *Geol. Surv. Can. Open File* 603, Scale 1:20000.
- Read, P.B., 1990. Mount Meager Complex, Garibaldi Belt, Southwestern British Columbia. *Geosci. Can.* 17, 167–170.
- Sherrod, D.R., Smith, J.G., 1990. Quaternary extrusion rates of the Cascade Range, Northwestern United States and Southern British Columbia. *J. Geophys. Res.* 95, 19465–19474.
- Stasiuk, M.V., Russell, J.K., Hickson, C.J., 1996. Distribution, nature, and origins of the 2400 B.P. eruption products of Mount Meager, British Columbia: linkages between magma chemistry and eruption behaviour. *Geol. Surv. Can. Bull.* 486.
- Stewart, M.L., 2002. Dacite block and ash avalanche hazards in mountainous terrain: 2360 yr. BP eruption of Mount Meager, British Columbia. MSc Thesis. University of British Columbia, Vancouver, B.C. p. 109.
- Stewart, M.L., Russell, J.K., Hickson, C.J., 2002. Revised stratigraphy of the Pebble Creek Formation, British Columbia: Evidence for interplay between volcanism and mountainous terrain. *Geol. Surv. Can. Curr. Res.* 2002-E3, pp. 1–7.
- Stewart, M.L., Russell, J.K., Hickson, C.J., 2008. Geology, Pebble Creek Formation, British Columbia. *Geol. Surv. Can. Open File* 5533, Scale 1:10000.
- Suzuki, T., Takahashi, K., 1981. An experimental study of wind abrasion. *J. Geol.* 89, 509–522.
- Thirumalai, K., 1969. Process of thermal spalling behaviours in rocks – an exploratory study. In: The 11th U.S. Symposium on Rock Mechanics. USRMS, Berkeley, CA, pp. 705–727.
- Tullis, J., Yund, R.A., 1977. Experimental deformation of dry Westerly granite. *J. Geophys. Res.* 82, 5705–5718.
- Varekamp, J.C., 1993. Some remarks on volcanic vent evolution during plinian eruptions. *J. Volcanol. Geotherm. Res.* 54, 309–318.
- Verhoef, P.N.W., Kuipers, T.J., Verwaal, W., 1984. The use of the sand-blast test to determine rock durability. *Bull. Int. Assoc. Eng. Geol.* 29, 457–461.
- Walker, G.P.L., Wilson, L., Bowell, E.L., 1971. Explosive volcanic eruptions – 1. The rate of fall of pyroclasts. *Geophys. J. R. Astron. Soc.* 22, 377–383.
- Westgate, J.A., Dreimanis, A., 1967. Volcanic ash layers of Recent age at Banff National Park, Alberta, Canada. *Can. J. Earth Sci.* 4, 155–161.
- Wilson, L., Sparks, R.S.J., Walker, G.P.L., 1980. Explosive volcanic eruptions – IV. The control of magma properties and conduit geometry on eruption column behaviour. *Geophys. J. R. Astron. Soc.* 63, 117–148.